ELSEVIER

Polymer 40 (1999) 5469–5478

polymer

Morphology development during phase inversion of a PS/PE blend in isothermal, steady shear flow

Nicole D.B. Lazo, Chris E. Scott*

Department of Materials Science and Engineering, Massachusetts Institute of Technology, Cambridge, MA 02139, USA

Received 27 July 1998; received in revised form 5 November 1998; accepted 8 November 1998

Abstract

The morphological changes occurring during the phase inversion of a polystyrene/polyethylene blend subjected to isothermal, steady shear flow are investigated and characterized. The isothermal, steady shear flow field provides a well-defined thermal and flow history. This contrasts with previous work on phase inversion, which was conducted in complex flow fields with large temperature gradients. The well-defined flow field permits a more detailed examination of the sequence of morphological changes during phase inversion than was accomplished previously. Both components are observed to initially deform into a sheet morphology. At strains of 200–780, the (initially continuous) minor component begins to break up, allowing the (initially dispersed) major component to coalesce. The blend becomes co-continuous around strains of 330–1500. At strains of 500–2000, the major component continues coalescing. The minor component breaks up into fibers and drops at strains of 800–3000. Breakup of the minor-component sheets is not observed until the sheets are less than 1 μm thick. Deformation and breakup of the initially dispersed phase is observed in this shear flow field, despite a viscosity ratio in excess of 10. For the system studied here, phase inversion does not occur under no-flow conditions.

Keywords: Phase inversion; Polymer blend; Shear flow

1. Introduction

Manufacturing blends of commercial polymers is often a faster, more cost-effective means of achieving a desired set of properties than synthesizing new polymers. Because blend performance depends crucially on the morphology, understanding the development of a blend's morphology during the manufacturing operation, and thus the morphology's dependence on processing conditions, is critical for process design. Commercial blends are generally produced in twin-screw extruders or intensive batch mixers where the polymers simultaneously undergo heating and a complex combination of shear and extensional flows that yield the target morphology. Modeling such complex flow fields in their entirety is beyond the capability of current computing resources. Therefore, efforts are focused on discovering and understanding the key mechanisms of morphological transformation in these processes and on how these mechanisms to contribute to the final blend morphology.

For processes such as intensive batch mixing and twin-screw extrusion, which involve dissipative mix-melting, Shih et al. [1] have classified the rheological changes which a single polymer experiences into four sequential rheological states:

1. elastic solid pellets;
2. softened and deformed pellets;
3. transitional material;
4. viscoelastic fluid.

When compounding polymer blends, each component individually passes through these four stages at different rates. The relative rates at which components change from solid pellets to viscoelastic fluids determine the morphology development of the blend. Shih [2,3] found that when the lower-concentration (or minor) component becomes a viscoelastic fluid much faster than the higher-concentration (or major) component does, an intermediate morphology consisting of the major component suspended in a continuous matrix of the molten minor component results. With further processing, the major component eventually reaches the viscoelastic fluid stage and a phase inversion occurs as illustrated schematically in Fig. 1. The major component becomes the continuous phase in which the minor component drops are finely dispersed, provided the blend's minor component concentration is sufficiently low. This phenomenon was first observed in a blend of 80/20 polyarylate/ethylene acrylic rubber [2].

* Corresponding author.

0032-3861/99/$ - see front matter
PII: S0032-3861(98)00792-7

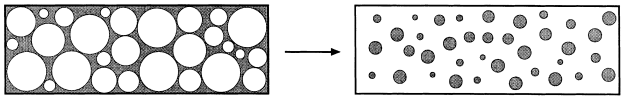

Fig. 1. Schematic illustration of phase inversion.

Shih proposed the following sequence of morphological changes during phase inversion:

1. The minor component forms the continuous phase in which closely packed pellets of the major component are suspended.
2. The major component begins to be dispersed in the minor component as the surfaces of the major-component pellets begin to soften and are sheared off from the solid core.
3. The major component continues to be dispersed in the minor component until the percolation threshold is reached. The percolation threshold is the minimum concentration at which a component forms a continuous path across the sample.
4. The blend phase inverts.

Shih confirmed this hypothesis in later work [4]. The transmission electron micrographs he reported only show a two-dimensional slice of the sample. Thus, it is uncertain whether the components exhibited a continuous/dispersed or a co-continuous morphology. However, his results do show that the dimension of the major component was reduced from its original size of 3 mm (solid pellets) to 5–20 μm (molten particles) when the major component first began to soften. It was further reduced to approximately 1 μm (molten particles) before phase inversion occurred. After phase inversion, the dispersed minor-component particles had a mean size of 0.7 μm.

Sundararaj and colleagues [5] expounded further on the mechanism of phase inversion. They compounded reactive and nonreactive blends of 80/20 polyarylate/ethylene–ethyl acrylate rubber, 80/20 polyamide 6,6/polystyrene and 80/20 polystyrene/ethylene propylene rubber. These blends were processed in an intensive batch mixer and examined via scanning electron microscopy after selective dissolution of the minor component. They found that the softened surfaces of the major-component pellets pulled off the solid core as sheets. These sheets broke into irregular pieces, some of them very small, that then appeared to coalesce together. Beyond a critical concentration of the softened or molten major component, the blend underwent phase inversion.

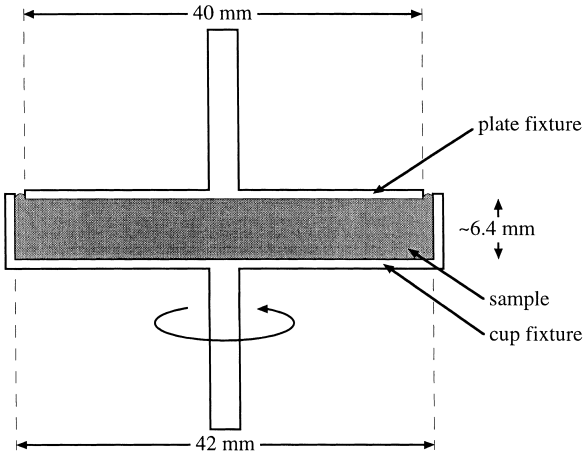

Fig. 2. Schematic diagram of the cup-and-plate fixture used in this study.

The previous work by Shih [4] and Sundararaj et al. [5] provides some insight into how phase inversion occurs during dissipative mix-melting. As the major component melts, it becomes dispersed in the minor component as either sheets or drops. As processing continues, the smallest dimension, termed the characteristic dimension, of the major-component morphology decreases in size before the major component coalesces and induces phase inversion. Sundararaj et al. [5] also inferred that phase inversion occurs once the melt concentration of the major component reaches the percolation threshold. It should be noted that the blend components in both studies were heated from room temperature to well above their transition temperatures during compounding in an intensive batch mixer. The simultaneous melting, shear deformation and elongational deformation occurring in these studies leave some fundamental questions unanswered. First, will phase inversion occur in purely shear flow, or only in the combined shear/elongational flows experienced in intensive mixers and twin-screw extruders? If so, will the morphological changes differ? Further, knowledge of the morphological changes that occur during phase inversion is still very general. What are the details of these changes? Is the major-component melt concentration alone the sufficient and necessary criterion for phase inversion? Can phase inversion be predicted by the total strain experienced by a blend? Some of these questions are addressed in this study.

The primary aim of this work is to study the phase inversion process isothermally in a well-defined steady-shear flow field. This is in contrast to previous work [1–8], which has focused on nonisothermal processes with complex flow fields. The emphasis of this work is on identifying the changes in morphology that occur during the phase inversion process. In addition, the progress of this transformation as a function of the total strain to which the sample is subjected is determined. To meet these goals, sample disks are prepared with a specific initial morphology: major-component pellets suspended in a continuous minor-component matrix. These samples are heated to the desired temperature in a strain rheometer and then subjected to steady shear flow in the parallel-disk fixture illustrated in Fig. 2 to induce phase inversion.

2. Experimental method

The materials used were commercially available polystyrene (PS) and polyethylene (PE) from Amoco and Dow Chemical, respectively. Their relevant thermal and

Table 1
Thermal and rheological properties of materials used

Polymer	Supplier	Softening/ melting temp (°C)	Viscosity at 0.5 s^{-1} and 180°C (Pa s)	Storage modulus at 0.5 s^{-1} and 180°C (Pa)
PS	Amoco	103 (T_g)	57,000	2,300
PE	Dow Chemical	129 (T_m)	4,000	700

rheological properties are summarized in Table 1. The transition temperatures were determined using differential scanning calorimetry and the melt viscosities and storage moduli via parallel-plate rheometry. Materials selection was based on several criteria. First, the transition temperatures had to be higher than room temperature to prevent the morphology from changing after processing. Second, it was necessary that a solvent for one component not dissolve or swell the other component, because the morphology was to be deduced by selectively dissolving one component and examining the remaining polymer. Third, the viscosity ratio, defined as the ratio of the major-component viscosity to the minor-component viscosity, of the blend had to fall within an operating window. Running blends with too high a viscosity ratio caused a significant amount of the blend to seep out of the experimental apparatus through the gap between the top fixture and the wall of the bottom fixture shown in Fig. 2. However, the sample preparation technique required the viscosity ratio to be greater than one at the molding temperature. Finally, it was desirable to use a system that had been extensively studied in a batch mixer for comparison with the results of this study. The detailed investigation of Scott and Joung [6] on phase inversion in the PS/PE system led to the selection of the PS/PE blend used for this study. The blend has a PS-to-PE viscosity ratio of 14 at the representative strain rate of 0.5 s^{-1}, a PS-to-PE viscosity ratio of 39 at the representative shear stress of 11,000 Pa, and methylene chloride selectively dissolves polystyrene. The elasticity ratio of PS to PE is 3 and the interfacial tension between PS and PE was reported to be 5 mN/m [9,10].

The blend composition for all runs was 85% PS and 15% PE. Selection of the blend composition was based on two opposing criteria. A low concentration of PE was required to obtain a post-processing morphology of PE dispersed in a continuous matrix of PS. However, the higher the PE concentration, the easier it was to ensure that the PE would be continuous and completely surround the PS pellets in the initial sample morphology. The PE concentration of 15% was chosen because, based on batch mixer runs, it was the highest PE concentration in which the final morphology was primarily PE dispersed in PS.

The 6.5 mm thick × 40.8 mm diameter disk samples of PS pellets dispersed in a continuous PE matrix were carefully prepared by compression molding. Prior to molding, the polymers were dried overnight in a vacuum oven at

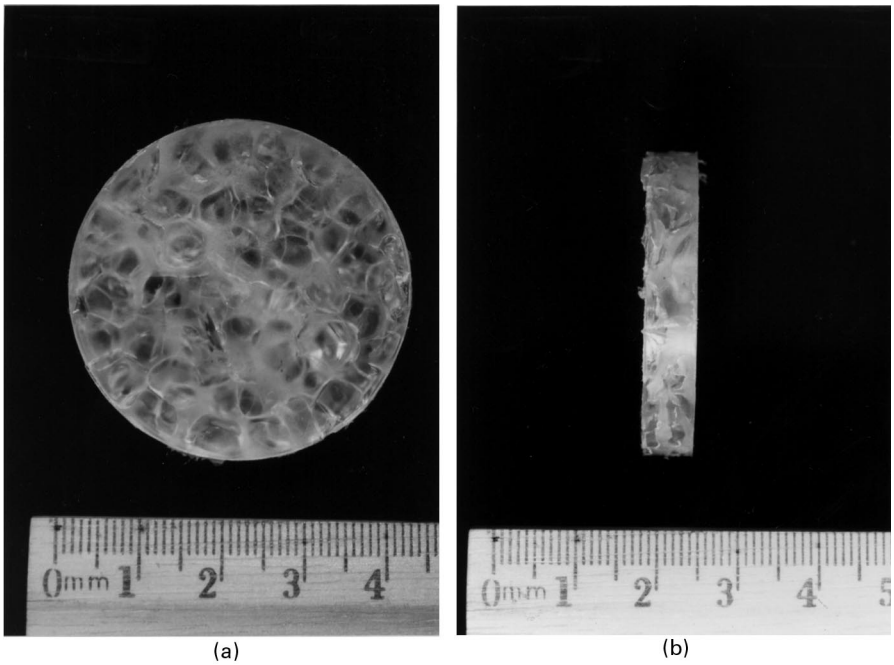

Fig. 3. Photographs of the (a) top view and (b) side view of a typical disk sample. The small tick marks on the ruler are 1 mm apart.

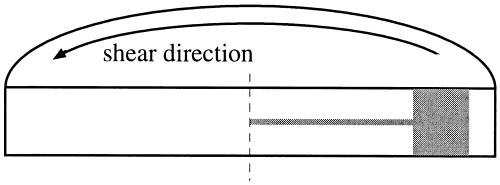

Fig. 4. Schematic diagram of the fracture surface relative to the disk sample. The grey regions are those examined at a magnification of 200 ×.

70°C. Each sample was prepared with 8 g (85% PS, 15% PE) of polymer. The minor phase polymer, PE, was first pressed into paper-thin disks roughly the diameter of the mold. One of these disks was then used to line the bottom of the heated mold and was topped with a pellet-thick layer of PS. On this was layered another PE disk, which was heated until it melted. The PE disk was then shaped with tweezers to ensure that PE surrounded each of the PS pellets. The layering was repeated twice until the mold was filled. The pressure on the mold was gradually increased to 250 bar, then held for about 3 minutes. The mold was subsequently unloaded and air-cooled. After the flash around the sample was removed, the samples weighted about 7.3 g. The composition of the final samples was confirmed by dissolution and reprecipitation of a representative disk. Using this molding technique, it is possible to prepare samples that, based on visual examination on a light table, are devoid of bubbles. However, this technique is limited to blends where the minor component is less viscous than the major component at the molding temperature. Otherwise, it is difficult to ensure that the major component is dispersed. Photographs of the top and side views of a typical sample are shown in Fig. 3.

The samples were subjected to steady shear flow in a Rheometrics ARES 600 strain rheometer using the cup-and-plate geometry illustrated in Fig. 2. The run temperature was 180°C and the strain rate at the rim of the plate was 0.5 s^{-1}. The initial capillary number based on the size of the PS pellets is approximately 1000. This indicates that the interfacial tension forces will not be important until the PS domain sizes are substantially reduced. To ensure that the sample had reached thermal equilibrium prior to the start of the run, the chamber was gradually heated to the setpoint temperature over a half-hour, then the gap was fixed — requiring the chamber to be opened briefly — and the chamber was held at the setpoint temperature for another half-hour before the run was begun. Runs producing total strains of 100, 500, 1000, and 4000 at the rim of the plate were conducted. In addition, a zero-strain sample was given the same pre-run treatment as the other samples and was held at 180°C under no-flow conditions for 2000 s after the start of run. This run time was chosen because it is equal to that of the 1000-strain sample. At the end of each run, the cup-and-plate fixture was removed from the rheometer and quenched in liquid nitrogen. This unloading procedure took about 1 minute. This is less than the time for Tomotika breakup because of thermally induced distortions [11,12]. After complete quenching, the cup was reheated to 135°C until the material in contact with the fixture softened and the sample could be removed from the fixture.

The samples were fractured into two halves in the radial direction at cryogenic temperatures, as shown in Fig. 4. Polystyrene was selectively dissolved from one half of each sample using methylene chloride in Soxhlet extraction apparatus. The exposed polyethylene and the unexposed second half of each sample were examined in an Electroscan EM-3 environmental scanning electron microscope. Each sample was scanned at a magnification of 200×. Each significant morphological feature detected was studied higher magnification.

3. Deformation field in the sample

There are significant differences between simple shear flow and the flow field generated in this study's experiments. A homogeneous material between infinite parallel plates undergoes simple shear flow. However, in these experiments, the blend is inhomogeneous and the geometry is cup-and-plate.

As a result of the cup-and-plate geometry, the flow field can be divided in two regions. In the region close to the center of the sample, the strain rate increases linearly with the radial coordinate and is independent of the axial coordinate. In the region close to the wall of the cup fixture, the strain rate initially increases with the radial coordinate, then attains a maximum and decreases to zero at the wall. In addition, the strain rate depends on the axial position. The velocity field for a Newtonian fluid in a cylindrical cavity with a rotating top plate was calculated for representative Reynolds numbers of 10^{-7}–10^{-6} using NEKTON™ 2.85. Resulting from the wall in the cup fixture, the tangential velocity, ν_θ, close to the wall is not a linear function of the axial coordinate z. The model predicts a shear-rate deviation of 10% at a radial distance of 14 mm and a deviation of 50% at a radial distance of 18 mm.

The strain-rate variation was taken into account when examining the sample morphologies in three ways. First, data from farther than 18 mm from the sample disk's center were excluded from the analysis, as shown in Fig. 4. Second, in the region where the strain rate depends on axial position (i.e. between 14 and 18 mm from the center), the entire fracture surface was examined. Third, morphologies having the same total strain but different strain rates were compared. These examinations showed that the morphology is independent of the strain rate for the strain rates used in this study.

In addition to the strain-rate variation, the blend itself is inhomogeneous. Thus, another concern is the homogeneity of blend deformation, particularly given the magnitude of the domain sizes in the blend relative to the gap between the plates. With two components of differing viscosities, it

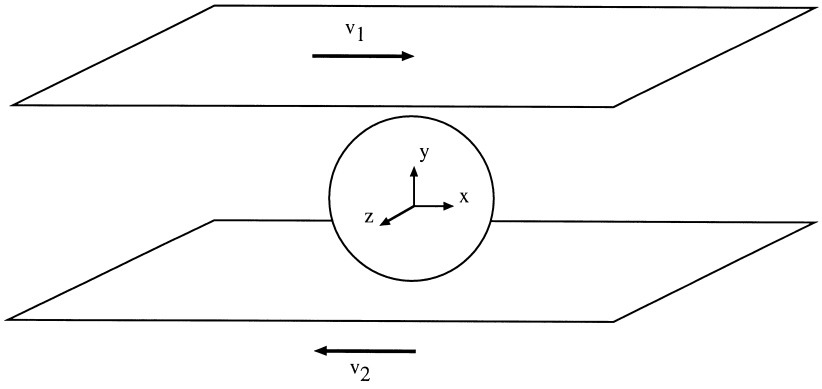

Fig. 5. Schematic diagram of affine deformation of a spherical pellet in simple shear flow between infinite parallel plates.

likely that most of the deformation occurs in the lower-viscosity component. To confirm that the higher-viscosity PS was deforming, a sample with a pillar of dyed PS located about 4 mm from the edge of the disk was made. The section of the sample with the dyed PS pillar was prepared by layering half of the paper-thin PE disks, the PS pillar, then the remaining PE disks, instead of the alternating layers of thin PE disks and PS pellets. This sample was run under the same conditions as the other samples to a total strain of 12 at the rim of the top plate. The PE-PS pillar-PE sandwich spanned the entire sample thickness. The PS pillar is expected to occupy 84% of the sample thickness, corresponding to the PS volume fraction in the sample. Affine deformation of this sandwich morphology should yield a longer, thinner structure with the PS still occupying 84% of the total length. The strain of 12 corresponded to a 225° rotation of the bottom fixture. The dyed PS traced an arc of 160°, which is 71% of the total rotation or, equivalently the dyed PS occupied 71% of the total length of the sandwich structure. This indicates that, while PS deforms, the blend does not deform affinely. This dyed pillar experiment also shows that the no-slip boundary condition as assumed in the NEKTON^{TM} flow simulation is valid.

4. Limiting case of affine deformation

The morphology produced by affine deformation of a blend with zero interfacial tension is an important limiting case for comparison with experimental results. Consider a spherical pellet with radius R in a continuous fluid between two parallel plates. As shown in Fig. 5, flow is in the x-direction, parallel to the plates; the velocity varies in the y-direction; and the z-direction is neutral. The coordinate system's origin is placed at the center of the pellet so that $v_x = 0$ at $y = 0$. The plate is moving in the $+x$-direction at a velocity v_1; the bottom plate moves in the $-x$-direction at a velocity v_2. If the blend deforms affinely, $v_y = v_z = 0$ and $v_x = \dot{\gamma} y$. A point P on the surface of the pellet has initial coordinates at:

$$x = x_0, \tag{1a}$$

$$y = y_0, \tag{1b}$$

$$z = z_0, \tag{1c}$$

where

$$x_0^2 + y_0^2 + z_0^2 = R^2. \tag{1d}$$

After an elapsed time t, each point in the sphere will move a distance in the x-direction of $\dot{\gamma} t y$ or γy. Thus, the point P will move to:

$$x = \gamma y + \sqrt{R^2 - y_0^2 - z_0^2} \tag{2a}$$

$$y = y_0, \tag{2b}$$

$$z = z_0. \tag{2c}$$

A constant-x slice of the deformed sphere is equivalent to the fracture surfaces observed in this study. At $x = 0$, the maximum width of the deformed sphere in the z-direction is $2R$; its maximum thickness in the y-direction is $2R/\sqrt{1 + \gamma^2}$. This yields a width-to thickness ratio, or aspect ratio, of $\sqrt{1 + \gamma^2}$. It can be shown that on a random y-z plane fracture surface the deformed spheres would have the same width-to-thickness ratio as at $x = 0$.

A homogeneous material deforms affinely. In this study, the blend components are immiscible and have different viscoelastic properties. Because of the resulting surface tension, as well as viscosity and elasticity inhomogeneities, the blend's morphology is expected to differ from the affine-deformation result. Qualitatively, the surface tension between the PS and the PE should cause the aspect ratio of the PS pellets to decrease in order to reduce its surface area. The greater viscosity and elasticity of the PS would further decrease its aspect ratio from the affine-deformation result [13–16]. This was confirmed by the dyed-PS-pillar experiment. Further, given the viscosity and elasticity ratios of this blend, the PS pellet is not expected to widen in the z-direction as a result of elastic forces [17].

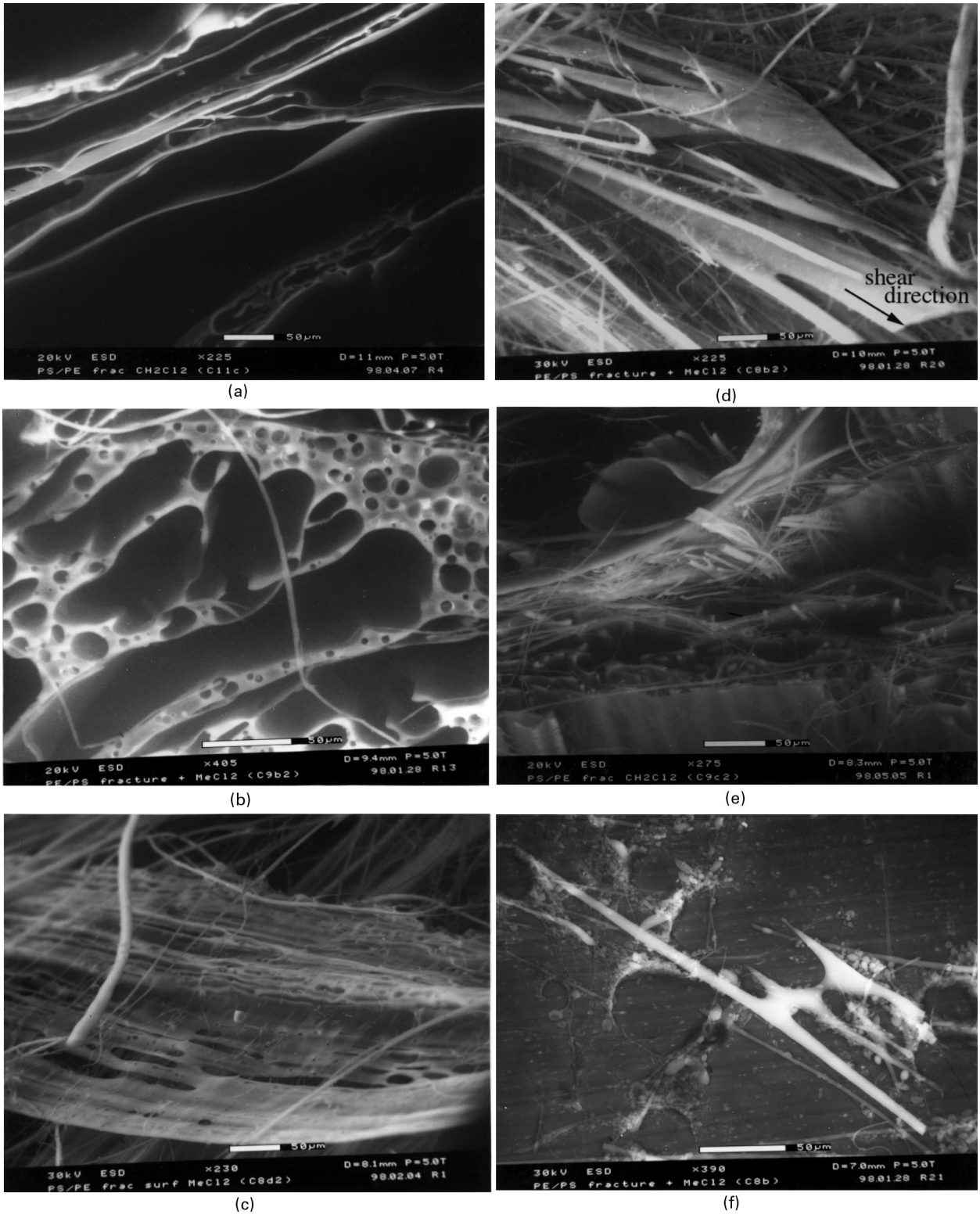

Fig. 6. Micrographs of morphologies observed at the following strains: (a) 50, (b) 200, (c) 330–3500, (d) 500–3500, (e) 500–3500, (f) 1000–3500. The micrographs show the fracture surfaces after the PS was dissolved using methylene chloride. The PE dispersed in PS, e.g. drops and fibers, likely moved from their original positions when the PS was dissolved.

5. Results and discussion

Selected micrographs of the observed morphologies are shown in Fig. 6. All the micrographs are of fracture surfaces perpendicular to the direction of flow as illustrated in Fig. 4. The PS was dissolved away, leaving PE. Note that any PE dispersed in PS, such as drops and many fibers, likely moved from its original location when the PS was dissolved.

The morphology pictured in Fig. 6a corresponds to a strain of about 50. It consists of PE completely encapsulating PS sheets. The PS and PE sheets vary in thickness, both within the sheet and between the sheets. The PS sheet sizes, in particular, vary widely from about 50 μm wide × 20 μm thick to more than 500 μm wide × about 120 μm thick. The PE sheet thicknesses vary between 3 and 15 μm. Sheet breakup and coalescence are shown in Fig. 6b. At a strain of about 200, PE is the continuous phase and the large, roughly rectangular shapes are PS sheets; the holes with almost circular cross-section correspond to PS drops and ellipsoids. Some of the PS sheets have begun to coalesce and where they have, a slight thickening of the recoiling PE sheet can be seen. Some of the PE has broken into fibers and drops.

Fig. 6c, taken at strains of about 330–3500, captures hole formation and growth in a PE sheet. Rather than growing isotropically, the holes lengthen preferentially in one direction and form slits. Based on the orientation of the holes relative to the fracture surface, Fig. 6d clearly shows that the preferred direction for hole growth is the shear direction. Also pictured in Fig. 6d are PE strands formed by the extensive breakup of the PE sheets. These strands, observed at strains of 500–3500, are shown in cross-section at the bottom of Fig. 6e. Although the thinner PE fibers have circular cross-sections, the thicker strands have distinctly elliptical cross-sections. The alignment of the fracture surfaces of the strands in Fig. 6e implies that the PE strand network is continuous in three dimensions. If the strands were one-dimensional, they would have slid apart after the PS was dissolved. If the strand network were continuous in only two dimensions, the sheets would have slid apart like a deck of cards. In either case, the fractured ends would not be aligned. Many PE drops and fibers can be seen in Fig. 6c–e, indicating that some regions of the sample have fully phase inverted.

Minor-component drops 2–5 μm in diameter were present in the largest-strain morphology (strain = 1000–3500) of this study, but so were larger minor-component structures, as shown in Fig. 6f. The post-phase-inversion, minor-component domains include PE drops, ellipsoids, fibers, and fragments of the PE strand network. The pictured fragment bordered four holes; strands separating the holes have broken off as the PS coalesced. Note that the PE fragment is significantly thicker than the PE drops and fibers. This is because of hole growth and the resulting PE recoil. This PE fragment would have to be thinned for further breakup to occur.

The observed sequence of morphological changes during phase inversion in this system is summarized in Fig. 7. Each portion of Fig. 7 illustrates the sample morphology at a given strain. As a result of the local variations in both the PE concentration and the initial PE domain size, a particular morphology is observed over a range of total strains. The orientation of the flow field relative to the illustrations is defined in Fig. 7a. The velocity is in the *x*-direction; the velocity varies in the *y*-direction; and the *z*-direction is neutral. The grey regions represent PE domains; the white, PS domains.

At zero strain, each softened, 2–3 mm-thick pellet of PS is coated with the molten PE (Fig. 7a). As the blend is sheared, the pellets deform into sheets (Fig. 7b). At a strain of about 50 (Fig. 7c), there are two size scales observed for the sheets: some sheets are about 100 μm wide × 20 μm thick; others are more than 1 mm wide × 100 μm thick. For a strain of 50 and an initial pellet size of 2–3 mm, affine deformation of a zero-interfacial-tension blend predicts a maximum thickness of 40–60 μm and an aspect ratio of 50. This predicted sheet thickness is in the range of thicknesses observed in Fig. 7c. However, there are sheets that are considerably thicker than 40–60 μm and the aspect ratio of these observed sheets is only 5–10. This finding is in agreement with the expected deviation of the experimental results from the affine-deformation prediction because of viscosity and elasticity inhomogeneities, as well as surface tension.

By a strain of 170–200, the remaining PS sheets are 100 μm wide × 20 μm thick on average (Fig. 7d). In addition to the sheets, PS drops of 3–20 μm diameter are observed. The PS sheets and drops are separated by 1–10 μm-thick PE sheets. The mechanism for the formation of the PS drops has not yet been confirmed. However, a possible mechanism is the necking of the sheet and the subsequent breakup of the neck into satellite drops. Rumscheidt and Mason [18] observed this phenomenon in drop breakup of dilute blends sheared at comparable strain rates, although those blends had viscosity ratios lower than that of the PS/PE blend used here. However, Grace [19] reported that it is impossible to induce drop breakup in dilute blends with viscosity ratios greater than 3.5. This contrasts with the observed deformation and breakup of the dispersed PS pellets in this study despite a blend viscosity ratio of 14. It seems likely, however, that the extremely high concentration of the dispersed PS phase changes the apparent viscosity ratio of the blend. The system studied here is intermediate between a single PS drop in an infinite PE matrix and a PS drop coated with a thin PE layer in an infinite PS matrix. In the latter case, which more closely represents the system here, the PS drop experiences a higher apparent matrix viscosity than in the former. Thus, the ratio of the drop viscosity to the apparent matrix viscosity may be considerably less than 3.5, permitting drop breakup and satellite drop formation.

As the strain increases to a total of 200–780, the PE

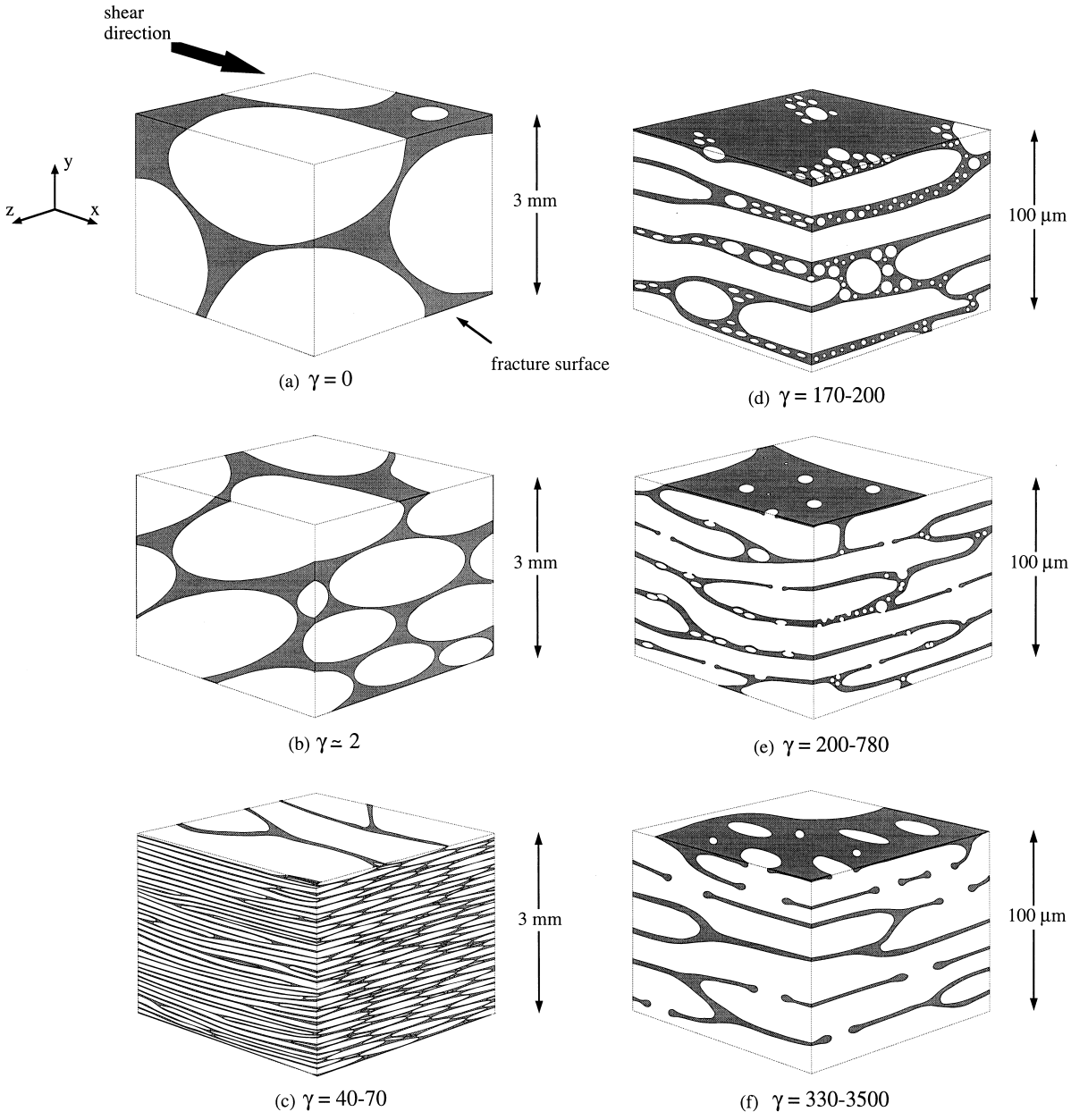

Fig. 7. Schematic illustration of the proposed sequence for phase inversion in steady shear flow.

sheets separating the PS domains thins to about 0.2 μm in some regions. This sheet thickness is similar to the critical drop separation for coalescence in the theory of Elmendorp and Van der Vegt [10]. They estimated that a typical polymer system would have a critical drop separation of 0.05 μm. Using the same approach, the polystyrene domains in this study are expected to coalesce when separated by 0.06 μm of PE. In contrast, Grizzuti and Bifulco [20] experimentally obtained a critical drop separation of 0.2 μm in polydimethylsiloxane/polyisobutylene blends.

Holes form in areas where the PE sheet becomes sufficiently thin (Fig. 7e). These holes only grow if, in doing so, the total energy of the system decreases. To a first-order approximation, the only relevant energy term is the surface energy. When a hole with radius r grows in a sheet of thickness t, the change in interfacial area is $2\pi tdr$-$2 \times 2\pi rdr$. A negative net change in area, and therefore in surface energy, requires $2r > t$. Therefore, holes grow only if their diameters exceed the sheet thickness. Thus, when the minor-component phase is thin, the probability increases that nucleated holes will grow, rather than shrink. Growth of the holes allows the PS regions on either side of the PE sheet to begin coalescing: drops coalesce with other drops and sheets, and sheets begin to coalesce with other sheets. The smallest holes observed in the PE sheets are 8 μm in diameter. Formation and growth of these holes entail the local removal of the minor component from the ruptured area. This results in a slight thickening of the

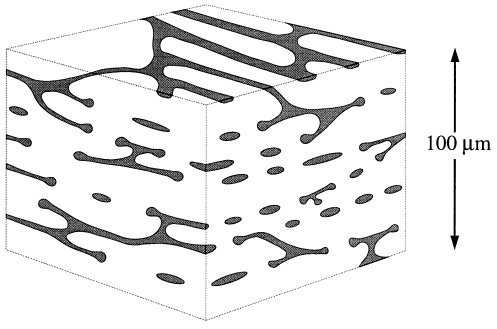

(g) γ = 500-3500

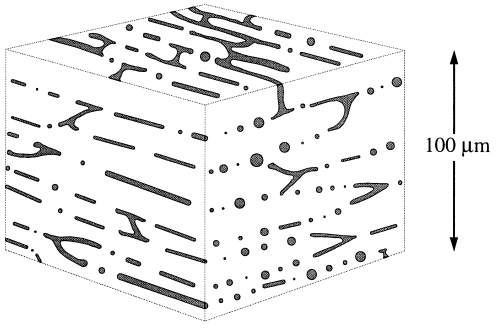

(h) γ = 800-3500

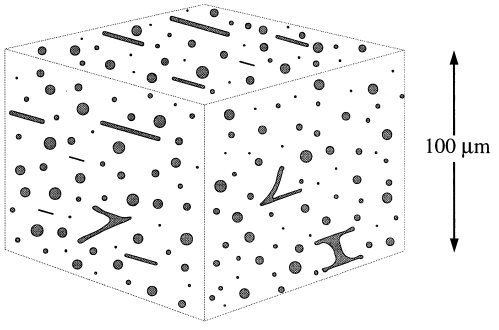

(i) γ = 1000-3500

Fig. 7. (*continued*)

minor-component sheet near the hole. Some of the minor component is not removed to the rim of the hole, but, instead, is trapped as drops in the major component as the major component coalesces.

As the strain reaches 330–3500, the holes in the PE sheets increase in number and lengthen in the direction of shear, remaining about 8 μm wide (Fig. 7f). The PE right at the edge of the holes is about 4 μm thick. With continued hole formation and growth (500–1000 strain), the minor-component sheets become 3-dimensional networks of flat strands that are oval in cross-section (Fig. 7g); the cross-sections measure 7 μm × 15 μm on average. Further strain thins these flat strands to axisymmetric 1–4 μm-diameter fibers (Fig. 7(h)), which eventually break up into 1–4 μm-diameter drops (Fig. 7i).

Comparison to Shih's work [4] is difficult because the transmission electron micrographs shown only yield two-dimensional morphological data. However, the clear trend in Shih's data is the decrease in the characteristic dimension of the major component before coalescence occurs. This study's data follow a similar trend as well; the major component deforms into sheets, which thin before coalescing. The characteristic dimension of the major component in Shih's shortest-mixing-time sample is 5–20 μm, which is the same range as that of the major-component drops in this study. Shih's longer-mixing-time samples have dispersed-phase characteristic dimensions about one-third that in this study's samples.

There is an important difference between the compounding method used in Ref. [5] and the method used here. Despite this, both approaches initially produce qualitatively similar morphologies. In Sundararaj et al.'s work, the major component simultaneously melts (or softens) and undergoes shear flow, thus causing sheets to separate from the solid pellet core. In this work, the components are heated to above their transition temperatures before the sample undergoes shear flow and the entire pellet deforms into sheets. Unfortunately, quantitative data of the sheet cross-section in [5] are unavailable for further comparison. After sheet formation, Sundararaj et al. observed sheet breakup into irregular shapes accompanied by coalescence. Again, Sundararaj et al.'s data does not include sheet-thickness information. However, the widths of the sheets (10–100 μm) and those of the finger-like extensions of the sheets (less than 8 μm) in their work are comparable to the widths of the sheets and drops observed in this study. There is evidence in Sundararaj et al.'s work of the formation of a minor-component network after further processing. This morphology is similar to the PE strand network reported here albeit with less regular cross-sections. Their structures are about 5–15 μm across in the narrower direction. This is comparable to the minor-axis length in the PE strand network's cross-section. The final morphology that Sundararaj et al. observed was of minor-component drops dispersed in the continuous major component. These drops had a range of diameters of about 1–10 μm. The presence in this study of the minor-component fibers and strand-network fragments, even at 3500 strain, is likely because of these samples experiencing less intense mixing than in Sundararaj et al.'s work.

Sundararaj et al. [5] inferred that phase inversion occurred once a critical melt concentration of the major component was reached. In this study, the major-component melt concentration was always above the critical concentration, but the sample did not actually phase invert until a strain of about 1000. The kinetics of phase inversion depends on the rate of hole nucleation in the PE sheets separating the PS regions. Straining the sample decreases the thickness of the PE sheets which, in turn, increases the hole nucleation rate. Thus, the major component's critical melt concentration is not the only factor governing phase inversion.

To thin the minor-component sheet and increase the hole

nucleation rate, the major component must deform in the flow field. Thus, phase inversion is expected to be more difficult to induce in blends with higher major-component viscosities and higher minor-component concentrations. This hypothesis agrees with the trends found in Refs. [6,7]. Further, phase inversion is not expected to occur in the disk samples under no-flow conditions because the PE sheets would be too thick in most regions to allow a large hole nucleation rate. This prediction is supported by the zero-strain sample, which did not phase invert after being annealed at 180°C for 40 min.

6. Conclusions

Phase inversion in isothermal steady shear flow was confirmed and the associated morphological changes characterized in detail. Initially, there is a simultaneous decrease in both components' characteristic dimensions. This is followed by an increase in size as the major component coalesces and the minor component recoils from ruptures. With increasing strain, the minor component continues to experience a cyclical decrease and increase in characteristic dimension until it reaches its final morphology of thin fibers and drops. These morphological changes occurred despite the dispersed phase being over 10 times more viscous than the continuous phase at the same strain rate. This result is likely because of the high concentration of the dispersed phase, which increased the apparent matrix viscosity. Finally, the data show that melt composition is not the only parameter governing the dynamics of phase inversion as previously hypothesized. Rather, the minor-component thickness, which influences the hole nucleation rate in minor-component sheets, should also be considered in any development of a phase inversion criterion.

Acknowledgements

The authors gratefully acknowledge the National Science Foundation, which funded this work and a research assistantship for N.D.B. Lazo under Award Number DMI-9624388. In addition, this work made use of MRSEC Shared Facilities supported by the National Science Foundation under Award Number DMR-9400334.

References

[1] Shih C-K, Tynan DG, Denelsbeck DA. Polym Eng Sci 1991;31:1670.
[2] Shih C-K. SPE ANTEC Conf. Proc. 1991;37:99.
[3] Shih C-K. Adv Polym Tech 1992;11:223.
[4] Shih C-K. Polym Eng Sci 1995;35:1688.
[5] Sundararaj U, Macosko CW, Shih C-K. Polym Eng Sci 1996;36:1769.
[6] Scott CE, Joung SK. Polym. Eng Sci 1996;36:1666.
[7] Ratnagiri R, Scott CE. Accepted by Polym Eng Sci
[8] Sundararaj U. Macromol Symp 1996;112:85.
[9] Elmendorp JJ, De Vos G. Polym Eng Sci 1986;26:415.
[10] Elmendorp JJ, Van de Vegt AK. Polym Eng Sci 1986;26:1332.
[11] Elmendorp JJ. Polym Eng Sci 1986;26:418.
[12] Huneault MA, Champagne MF, Luciani A. Polym Eng Sci 1996;36:1694.
[13] Torza S, Cox RG, Mason SG. J Colloid Interf Sci 1972;38:395.
[14] Elmendorp JJ, Maalcke RJ. Polym Eng Sci 1985;25:1041.
[15] Varanasi PP, Ryan ME, Stroeve P. Ind Eng Chem Res 1994;33:1858.
[16] Ghodgaonkar PG, Sundararaj U. Polym Eng Sci 1996;36:1656.
[17] Levitt L, Macosko CW, Pearson SD. Polym Eng Sci 1996;36:1647.
[18] Rumscheidt FD, Mason SG. J Colloid Sci 1961;16:238.
[19] Grace HP. Chem Eng Commun 1982;14:225.
[20] Grizzuti N, Bifulco O. Rheol Acta 1997;36:406.